NJC

ROYAL SOCIETY OF CHEMISTRY

PAPER

View Article Online
View Journal | View Issue

Cite this: *New J. Chem.*, 2024, **48**, 14884

Spectroscopically labelled hydroxylamino-triazine (BHT) siderophores toward the quantification of iron(III), vanadium(V) and uranium(VI) hard metal ions†

Angelos Amoiridis,[a] Michael Papanikolaou,[a] Chryssoula Drouza,[b] Themistoklis A. Kabanos *[c] and Anastasios D. Keramidas *[a]

Received 7th June 2024,
Accepted 29th July 2024

DOI: 10.1039/d4nj02645d

rsc.li/njc

Based on the strong binding properties of hydroxylamino-1,3,5-triazine (BHT) for hard metal ions, a novel spectroscopically labelled triazine-hydroxylaminato ligand, *N*,*N*′-(6-(9*H*-carbazol-9-yl)-1,3,5-triazine-2,4-diyl)bis(*N*-methylhydroxylamine) (H_2cbht), was synthesized. Reaction of H_2cbht with Fe^{III}, V^V and U^{VI} resulted in the synthesis of $[U^{VI}O_2(cbht)(DMF)(MeOH)]$, **1**, $(PPh_4)_2([U^{VI}O_2(Hcbht)_2]\cdot 2[U^{VI}O_2(Hcbht)(cbht)])$, **2**, $(PPh_4)_2[(U^{VI}O_2)_3(\mu\text{-}cbht)_2(cbht)_2]$, **3**, $Na[V^VO_2(cbht)]$, **4**, and $(PPh_4)[Fe^{III}(cbht)_2]$, **5**. The complexes were characterized by X-ray crystallography showing strong chelation of the metal ions with the BHT chelating moiety H_2cbht. The DMSO/DMF solutions of the complexes were characterized by NMR, UV-vis and electrochemistry, confirming the high affinity of H_2cbht for Fe^{III}, V^V or U^{VI}. The luminescence properties of the carbazole group were retained in the BHT adduct of the H_2cbht ligand. Interaction of the metal ions with H_2cbht resulted in quenching of the luminescence of H_2cbht. Stern–Volmer plots of luminescence *vs.* concentration of the metal ions are linear and suitable for the determination of the concentration of metal ions in nM range concentrations. Benesi–Hildebrand plots show that the metal-to-ligand ratio is 1 : 1 while the formation of the metal complexes exhibits high association constants.

Introduction

The removal of hard metal ions (referring to the hard–soft acid base theory, HSAB) from the environment, human body, and radioactive wastes produced by nuclear industries and metal mining from seawater has motivated scientists toward the synthesis of new, strong and selective chelators, including siderophores.[1–27] A group of non-toxic siderophores, based on an *N*,*N*′-disubstituted bis(hydroxyamino)-1,3,5-triazine (BHT) moiety (Scheme 1), shows explicit preference to binding hard metal ions, such as Fe^{III}, Ti^{IV}, V^V, U^{VI} and Mo^{VI}.[3,10–14,28–31]

Highly sensitive and specific probes for various metal ions have been synthesised and intensively investigated by scientists due to their potential applications in environmental sciences and biological systems for understanding their roles in different chemical and biological processes.[32–53] In particular, the concentration of metal ions can be increased in humans through industrial pollution and war pollution; for example, using depleted uranium in ammunition,[18,54–57] release of unregulated metal ions in organisms connected to certain diseases[58,59] and the use of biologically active metal complexes as drugs. For example, vanadium complexes have shown such activity, mainly as antidiabetic and anticancer drugs.[60–78]

An advantage of BHT-type ligands is their easy modification by replacing the R group (Scheme 1) while keeping the same chelating moiety. The type of R group can directly influence the electron-donating ability of the chelator, thus modifying the electronic properties[31] of the coordinated metal ions. Subsequently, R groups with optical and/or electrochemical properties will provide BHT-type ligands with sensing capabilities.

The chelating group controls selectivity and affinity towards the metal ions. The selectivity and thermodynamic stability of H_2bihyat (Scheme 1) for $[V^VO_2]^+$ and $[U^{VI}O_2]^{2+}$ were found to be superior to those of other hard donor ligands, such as

[a] *University of Cyprus, Department of Chemistry, 2109, Nicosia, Cyprus. E-mail: akeramid@ucy.ac.cy*
[b] *Department of Agricultural Sciences, Biotechnology and Food Science, Cyprus University of Technology, Limassol 3036, Cyprus. E-mail: chryssoula.drouza@cut.ac.cy*
[c] *Department of Chemistry, Section of Inorganic and Analytical Chemistry, University of Ioannina, 45110 Ioannina, Greece. E-mail: tkampano@uoi.gr*

† Electronic supplementary information (ESI) available. CCDC 2360878 (**1**), 2360879 (**3**·DMF), 2360880 (**5**·9H_2O), 2360881 (**2**·MeOH·Et_2O·2H_2O), and 2360882 (**4**·3H_2O). For ESI and crystallographic data in CIF or other electronic format, see DOI: https://doi.org/10.1039/d4nj02645d

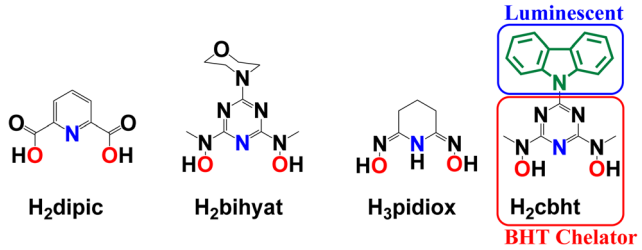

Scheme 1 Molecular drawings of H_2dipic, H_2bihyat, H_3pidiox and H_2cbht.

pyridine-2,6-dicarboxylic acid (H_2dipic; Scheme 1) and amidoxime (H_3pidiox, Scheme 1), indicating that BHT-type ligands are the best candidates for the development of sensors for these metal ions.

Herein, we describe the synthesis of *N*,*N*′-(6-(9*H*-carbazol-9-yl)-1,3,5-triazine-2,4-diyl)bis(*N*-methylhydroxylamine) (H_2cbht, Scheme 1), a carbazole covalent adduct with a BHT chelating group. The organic molecule H_2cbht retains the luminescence and redox properties of carbazole and is the first luminescent BHT ligand to be reported. Reactions of H_2cbht with $U^{VI}O_2^{2+}$, $V^{V}O_4^{3-}$ and Fe^{III} in organic solvents result in the synthesis of $[U^{VI}O_2(cbht)(DMF)(MeOH)]$, **1**, $(PPh_4)_2([U^{VI}O_2(Hcbht)_2]\cdot 2[U^{VI}O_2(Hcbht)(cbht)])$, **2**, $(PPh_4)_2[(U^{VI}O_2)_3(\mu\text{-}cbht)_2(cbht)_2]$, **3**, $Na[V^{V}O_2(cbht)]$, **4**, and $(PPh_4)[Fe^{III}(cbht)_2]$, **5**. The complexes were characterized in the solid state by X-ray crystallography. The speciation in solution and thermodynamic stability of the metal complexes were determined by 1D and 2D ^{1}H NMR spectroscopy and electrochemistry. The coordination of the metal ions to H_2cbht results in the quenching of luminescence. The Stern–Volmer graphs of the quenching of the luminescence are linear, indicating that the plots can be used for $U^{VI}O_2^{2+}$, $V^{V}O_4^{3-}$ and Fe^{III} quantification in nM level concentration. The large association constants calculated from the luminescence spectra confirm the high thermodynamic stability of the complexes.

Experimental section

All the chemicals were of reagent grade purity and were provided by Sigma-Aldrich unless otherwise stated. THF was dried over a sodium wire and distilled just prior to use.

n-BuLi in hexane is flammable and ignited in the presence of air.

Synthesis of 9-(4,6-dichloro-1,3,5-triazin-2-yl)-9*H*-carbazole (dctc)

To a solution of carbazole (2.84, 17 mmol) in dry THF (40 mL), a solution (2.5 M) of *n*-BuLi in hexane (6.8 mL, 17 mmol) was added over 10 minutes at −40 °C, under an argon atmosphere. The resulting mixture was stirred at room temperature for 30 minutes under argon flow and added to a stirred solution of cyanuric chloride (3.12 g, 17 mmol) in THF (40 mL) using a dropping funnel over 30 minutes at 0 °C. The red mixture was allowed to reach room temperature and then refluxed overnight. After that, the solvent was removed under reduced pressure and acetone (20 mL) was added to the red-white residue. The mixture was stirred for 30 minutes in an ice bath, and a white solid (4.82 g) was collected by filtration and used without further purification. Yield: 90% (based on carbazole). ^{1}H NMR ($CDCl_3$, 500 MHz, 25 °C) δ (ppm): 8.56 (2H, d, J = 8.43 Hz, carbazole), 7.99 (2H, d, J = 7.60 Hz, carbazole), 7.52 (2H, td, J = 7.22, 1.33 Hz, carbazole), 7.45 (2H, td, J = 7.40, 0.87 Hz, carbazole). ^{13}C NMR ($CDCl_3$, 125.7 MHz, 25 °C) δ (ppm): 171.42, 163.93, 138.63, 128.19, 127.93, 125.56, 120.25, and 119.36. IR(ATR): ν(BHT ring) 723, 758 1475, 1500, 1535 cm^{-1}. Elemental analysis of $C_{15}H_8Cl_2N_4$ (M_r = 315.2): found C, 56.99; H, 2.52; N, 17.83; calculated: C, 57.17; H, 2.56; N, 17.78.

Synthesis of *N*,*N*′-(6-(9*H*-carbazol-9-yl)-1,3,5-triazine-2,4-diyl)-bis(*N*-methylhydroxylamine) (H_2cbht)

To a stirred aqueous solution (2 mL) of *N*-methylhydroxylamine hydrochloride (1.33 g, 15.9 mmol), an aqueous solution (2 mL) of NaOH (0.630 g, 15.9 mmol) was added dropwise at 0 °C, and the resulting solution was slowly added to a solution of dctc (1.25 g, 3.97 mmol) in THF (20 mL) at 0 °C. Then, the solution was allowed to reach room temperature (25 °C) and refluxed overnight, after which a white solid was formed, which was filtered, washed with THF (5 mL) and distilled water (2 × 5 mL), and dried under vacuum to give 1.08 g of the ligand H_2cbht. Yield: 81% (based on dctc). ^{1}H NMR (DMSO-d_6, 500 MHz, 25 °C) δ (ppm): 9.90 (2H, s, N–OH), 9.12 (2H, d, J = 8.35 Hz, carbazole), 8.17 (2H, d, J = 7.69 Hz, carbazole), 7.49 (2H, td, J = 7.17, 1.31 Hz, carbazole), 7.37 (2H, td, J = 7.15, 0.87 Hz, carbazole), 3.45 (6H, s, N–CH_3). ^{13}C NMR (DMSO-d_6, 125.7 MHz, 25 °C) δ (ppm): 166.94, 163.91, 138.69, 126.71, 125.22, 122.47, 119.80, 118.09, and 38.51. IR(ATR): ν(BHT ring) 723, 758 1392, 1438, 1641 cm^{-1}. Elemental analysis of $C_{17}H_6N_6O_2$ (M_r = 336.4): found: C, 59.89; H, 4.85; N, 24.24; calculated: C, 60.71; H, 4.79; N, 24.99.

Synthesis of $[U^{VI}O_2(cbht)(DMF)(MeOH)]$, 1

H_2cbht (0.0760 g, 0.226 mmol) and triethylamine (63.0 µL, 0.452 mmol) were sequentially added to a stirred DMF (5 mL) solution of $[U^{VI}O_2(NO_3)_2(H_2O)_2]\cdot 4H_2O$ (0.113 g, 0.226 mmol), which yielded a dark brown solution. XRD quality single crystals of **1** (0.116 g) were obtained by layering methanol (6 mL) to an undisturbed brown solution. Yield: 74% (based on H_2cbht). ^{1}H NMR (DMSO-d_6, 500 MHz, 25 °C) δ (ppm): 8.95 (2H, d, J = 8.40 Hz, carbazole), 8.21 (2H, d, J = 7.70 Hz, carbazole), 7.55 (2H, td, J = 7.30, 1.50 Hz, carbazole), 7.38 (2H, td, J = 7.80, 0.80 Hz, carbazole), 3.79 (s, 6H, N–CH_3). ^{13}C NMR (DMSO-d_6, 125.7 MHz, 25 °C) δ (ppm): 162.34, 160.67, 159.46, 138.82, 126.71, 124.94, 122.12, 119.78, 117.34, and 38.20. IR(ATR): ν(BHT ring) 719, 752, 771, 1442, 1535, 1639 cm^{-1}, ν(U=O), 905 cm^{-1}. Elemental analysis of $C_{20}H_{23}N_7O_6U$ (M_r = 695.2): found: C, 34.39; H, 3.48; N, 13.99; calculated: C, 34.54; H, 3.33; N, 14.10.

Synthesis of $(PPh_4)_2([U^{VI}O_2(Hcbht)_2]\cdot 2[U^{VI}O_2(Hcbht)(cbht)])\cdot 2MeOH\cdot 2Et_2O\cdot 2H_2O$, 2, $\cdot 2MeOH\cdot 2Et_2O\cdot 2H_2O$ and $(PPh_4)_2[(U^{VI}O_2)_3(\mu\text{-}cbht)_2(cbht)_2]\cdot DMF$, 3·DMF

H_2cbht (0.0760 g, 0.226 mmol), $[U^{VI}O_2(NO_3)_2(H_2O)_2]\cdot 4H_2O$ (0.0570 g, 0.113 mmol) and triethylamine (378 µL, 2.71 mmol) were dissolved in 3 mL of DMF. To the stirred brown solution

solid, PPh_4Cl (0.169 g, 0.452 mmol) was added in one portion. The vapour diffusion of diethylether into the undisturbed brown solution resulted in two types of single crystals suitable for X-ray structure analysis. The needle-type crystals correspond to $(PPh_4)_2([U^{VI}O_2(Hcbht)_2]\cdot 2[U^{VI}O_2(Hcbht)(cbht)])\cdot 2MeOH\cdot 2Et_2O\cdot 2H_2O$ (complex **2**·MeOH·Et_2O·$2H_2O$) and the block-type crystals correspond to $(PPh_4)_2[(U^{VI}O_2)_3(\mu\text{-}cbht)_2(cbht)_2]\cdot DMF$ (complex **3**·DMF). The two complexes crystallize together, as shown in Fig. S1 (ESI†). The crystals were manually separated under a microscope. Yield: 0.0252 g, 17% (**2**·MeOH·Et_2O·$2H_2O$) and 0.0065 g, 6% (**3**·DMF). IR(ATR) of **2**: ν(BHT ring) 727, 754, 777, 1390, 1516 cm^{-1}, ν(U═O), 901 cm^{-1}. Elemental analysis of $C_{160}H_{160}N_{36}O_{24}P_2U_3$ (**2**·2MeOH·$2Et_2O$·$2H_2O$, M_r = 3729.29): found: C, 51.68; H, 4.51; N, 13.27; calculated C, 51.28; H, 4.30; N, 13.46. Elemental analysis of $C_{119}H_{103}N_{25}O_{15}P_2U_3$ (**3**·DMF, M_r = 2897.91): found: C, 49.87; H, 3.71; N, 11.92; calculated: C, 49.30; H, 3.58; N, 12.08.

Synthesis of $Na[V^VO_2(cbht)]\cdot 3H_2O$, **4**·$3H_2O$

To a stirred solution of H_2cbht (0.0760 g, 0.226 mmol) and triethylamine (63.0 µL, 0.452 mmol) in DMF (5 mL), an aqueous solution (2 mL) of NaV^VO_3 (0.0300 g, 0.226 mmol) was added, and the colour of the solution changed to yellow. The yellow solution was allowed to stand undisturbed at room temperature, and after 4 hours, XRD-quality orange crystals of complex **4**·$3H_2O$ (0.056 g) were obtained. Yield: 50% (based on H_2cbht). ^1H NMR (DMSO-d_6, 500 MHz, 25 °C) δ (ppm): 8.88 (2H, d, J = 8.50 Hz, carbazole), 8.19 (2H, d, J = 7.39 Hz, carbazole), 7.53 (2H, td, J = 7.32, 1.22 Hz, carbazole), 7.38 (2H, td, J = 7.08, 0.92 Hz, carbazole), 3.46 (s, 6H, N–CH_3). ^{13}C NMR (DMSO-d_6, 125.7 MHz, 25 °C) δ (ppm): 162.45, 157.34, 138.73, 126.85, 125.18, 122.48, 119.74, 117.69, and 35.82. IR(ATR): ν(BHT ring) 721, 758, 721, 1442, 1525, 1590, 1650 cm^{-1}, ν(V═O), 916 cm^{-1}. Elemental analysis of $C_{17}H_{20}N_6NaO_7V$ (M_r = 494.07): found: C, 41.38; H, 3.99; N; calculated: C, 16.87; 41.31; H, 4.08; N, 17.00.

Synthesis of $(PPh_4)[Fe^{III}(cbht)_2]\cdot 9H_2O$, **5**·$9H_2O$

H_2cbht (0.076 g, 0.226 mmol) and Et_3N (378 µL (2.71 mmol) were dissolved in 3 mL of DMF. $[Fe^{III}(NO_3)_3]\cdot 9H_2O$ 0.0460 g (0.113 mmol) was added to the DMF solution, and the colour of the solution turned dark purple. The addition of 1 mL of water to the stirred solution resulted in the formation of a small amount of a purple solid, which was re-dissolved by warming the solution to 100 °C. Then, the warm solution was slowly cooled to room temperature (20 °C) and left undisturbed for 3 days, after which small dark purple crystals (0.244 g) of **5**·$9H_2O$ suitable for X-ray structure analysis were precipitated. Yield: 75% (based on H_2cbht). Elemental analysis of $C_{58}H_{66}FeN_{12}O_{13}P$ (M_r = 1225.40): found: C, 57.42; H, 5.30; N, 13.88; calculated: C, 56.82; H, 5.43; N, 13.71.

Results and discussion

Synthesis of the ligand H_2cbht and complexes **1**–**5**·$9H_2O$

A slightly modified method reported in the literature[79] was used for the synthesis of dctc. The synthesis of dctc, shown in Scheme 2, is based on the nucleophilic substitution of cyanuric chloride and takes place in two steps. The first step involves the deprotonation of the cyclic amine nitrogen by a very strong base (*n*-BuLi), and the second step involves the substitution of one chlorine atom of cyanuric chloride with a nitrogen atom of the deprotonated carbazole. All glassware used for the synthesis of dctc was flame-dried, and all processes were performed under an inert atmosphere using high-purity argon flow. The synthesis of the ligand H_2cbht, depicted in Scheme 2, is based on the nucleophilic substitution of the two remaining chlorine atoms of dctc with *N*-methylhydroxylamine hydrochloride in a THF/H_2O solution previously neutralized with NaOH. The ligand H_2cbht is insoluble in water in the pH range 1–14.

The synthesis of uranium(VI) (**1**, **2**, and **3**) and vanadium(V) (**4**)/iron(III) (**5**) compounds is a one-pot synthesis, as shown in Schemes S1 and S2 (ESI†), respectively. Reaction of equivalent quantities of $U^{VI}O_2^{2+}$ and H_2cbht with two equivalents of Et_3N leads to the formation of complex **1**, while the reaction of $U^{VI}O_2^{2+}$ and H_2cbht in a molar ratio 1 : 2 in the presence of excess Et_3N (12 equivalents) and Ph_4PCl results in the formation of compounds **2** and **3**. ^1H NMR spectroscopy revealed that complexes **1**, **2** and **3** are in equilibrium in solutions containing $U^{VI}O_2^{2+}$ and H_2cbht. Addition of Et_3N and/or H_2cbht shifts the equilibrium towards **2** and **3**. Attempts to optimize the synthetic procedure in order to obtain **2** and **3** separately were unsuccessful. Reactions of $V^VO_4^{3-}$ or Fe^{III} with H_2cbht give only **4** ($V^VO_2^+$–$cbht^{2-}$ 1 : 1) or **5** (Fe^{III}–$cbht^{2-}$ 1 : 2), respectively. Complexes **1**–**5** are soluble in organic solvents, including DMF and DMSO.

Characterization of the complexes in the solid state

The synthesized compounds have been characterized in the solid state by Fourier transform infrared spectroscopy and X-ray

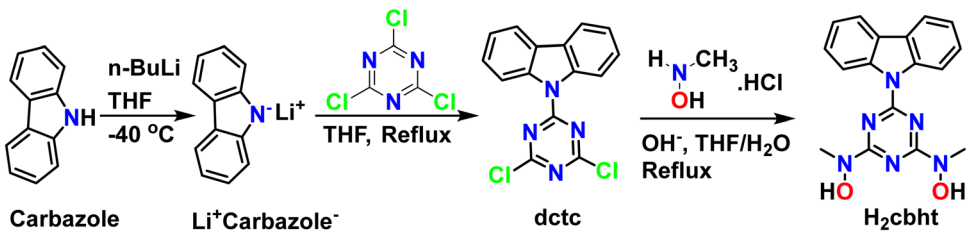

Scheme 2 Synthesis of organic molecules dctc and H_2cbht.

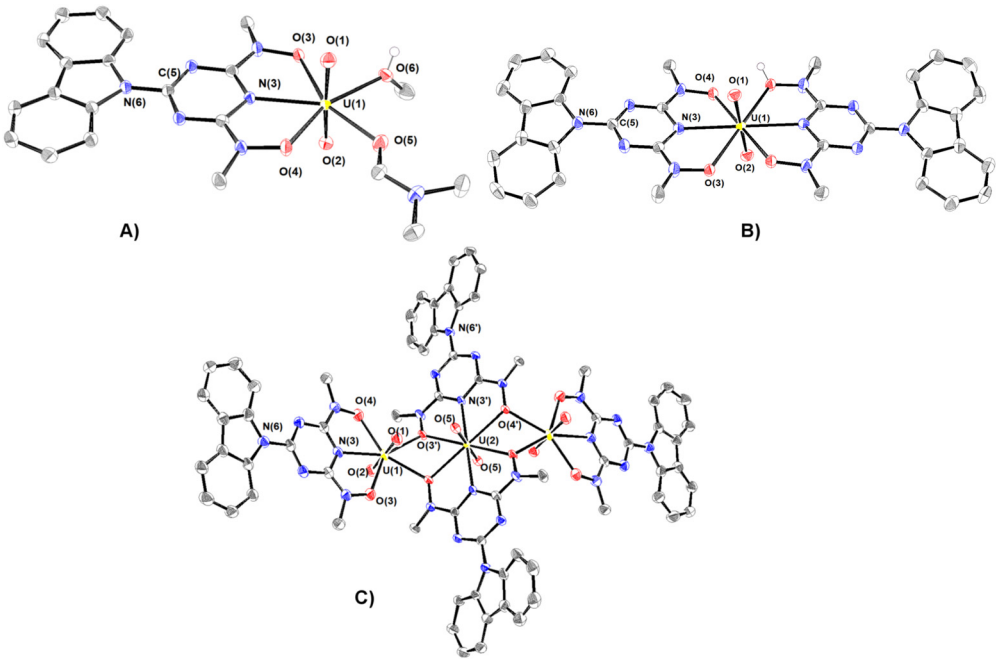

Fig. 1 ORTEP plots of **1** (A) and anions of **2** (B) (only one of the three uranyl molecules of **2** is shown for clarity) and **3** (C) with 50% thermal ellipsoids. Hydrogen atoms were omitted for clarity. Bond lengths (Å): (A) U–O(1) = 1.780(2), U–O(2) = 1.776(2), U–O(3) = 2.415(2), U–O(4) = 2.299(2), U–N(3) = 2.433(2), U–O(5) = 2.400(2), and U–O(6) = 2.382(2). (B) U–O(1) = 1.781(3), U–O(2) = 1.781(3), U–O(3) = 2.478(3), U–O(4) = 2.479(3), U–N(3) = 2.530(4). (C) U(1)–O(1) = 1.777(3), U(1)–O(2) = 1.793(3), U(1)–O(3) = 2.309(3), U(1)–O(4) = 2.319(3), U(1)–N(3) = 2.430(4), U(1)–O(3′) = 2.438(3), U(1)–O(4′) = 2.454(3), U(2)–O(5) = 1.781(3), U(2)–O(3′) = 2.466(3), U(2)–O(4′) = 2.503(3), and U(2)–N(3′) = 2.530(3).

crystallography. The infrared spectra and assignments of the characteristic peaks are shown in Fig. S2 (ESI†). A summary of the crystallographic data and the final refinement details for complexes **1**–**5**·9H_2O are provided in Tables S1 and S2 (ESI†). The interatomic distances and bond angles relevant to U^{VI}, V^{V} and Fe^{III} coordination spheres are listed in Tables S3 and S4 (ESI†). Ortep plots of the crystal structures of the uranium(VI) complexes **1**–**3**·DMF and **4**·3H_2O–**5**·9H_2O are shown in Fig. 1 and 2, respectively.

The uranium(VI) atom in complex **1** adopts a pentagonal bipyramidal structure, with two terminal oxido groups, O(1) and O(2) [d_{mean}(U═O) ∼ 1.778 Å], occupying the two axial positions, whereas the triazine nitrogen atom N(3), [d(U–N_{tr}) = 2.433 Å], two deprotonated hydroxylamine hydroxyls O(3) and O(4), and two oxygen atoms O(6) and O(7) of methanol and DMF molecules, lie in the equatorial plane. dU–O(3) (2.415 Å) is significantly longer than dU–O(4) (2.299 Å), reflecting the stronger *trans* effect of the DMF carbonyl than the methanol oxygen donor atoms.

The coordination environment of the three U^{VI} in the three hydrogen-bonded U^{VI}–$Hcbht^{-}$ molecules of complex **2** are hexagonal bipyramids with two oxido groups, O(1) and O(2) [d(U═O) = 1.781(3) Å] occupying the axial positions (Fig. 1(B) and Fig. S3, ESI†). The equatorial plane of the two uranium atoms is defined by the triazine nitrogen atom N(3) and the two hydroxylamine oxygen atoms O(3) and O(4) of $cbht^{2-}$ and $Hcbht^{-}$ ligands, whereas the third central U^{VI} is defined by the donor atoms of two $Hcbht^{-}$ ligands. Although some of the hydroxylamine oxygen atoms are deprotonated and others are

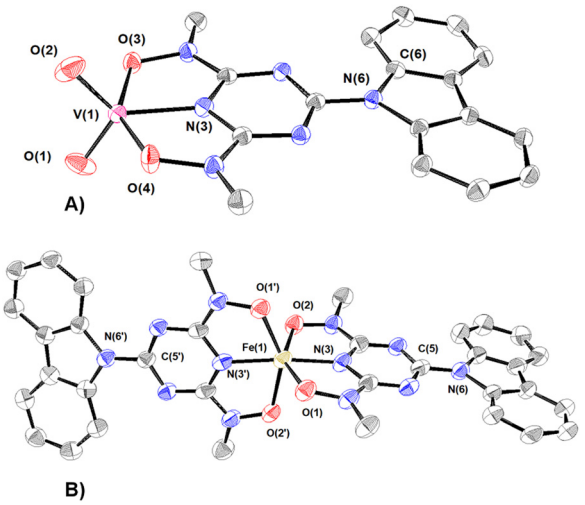

Fig. 2 ORTEP plots of the anions of **4** (A) and **5** (B) with 50% thermal ellipsoids. Hydrogen atoms were omitted for clarity. Bond lengths (Å): (A) V(1)–O(1) = 1.632(1), V(1)–O(2) = 1.631(1), V(1)–O(3) = 2.014(1), V(1)–O(4) = 1.971(1), and V(1)–N(3) = 1.984(1). (B) Fe(1)–O(1) = 2.029(3), Fe(1)–O(1′) = 2.043(3), Fe(1)–O(2) = 2.119(3), Fe(1)–O(2′) = 2.114(3), Fe(1)–N(3) = 1.980(3), and Fe(1)–N(3′) = 1.997(4).

not, the four U^{VI}–O_h bond lengths (∼2.479 Å) are indistinguishable. The protons of the hydroxylamine oxygen atom form a strong hydrogen bond [(H)O–O(4) = 2.549 (3) Å] with the deprotonated hydroxylamine oxygen atom [O(4)] of a neighbouring molecule, and *vice versa*, bringing the three uranyl molecules of **2** in close proximity, almost perpendicular to each

other [O(1)═U···U═O(1) torsion angle ∼115°]. The two equatorial triazine-hydroxylaminate parts of the ligands exert strong *trans* effect[31] to each other, resulting in significant lengthening of the four U^{VI}–O_h bonds in comparison with the corresponding U^{VI}–O_h bonds in **1**.

The structure of the anion of **3** (Fig. 1(C)) consists of two distorted pentagonal and a hexagonal bipyramidal uranyl unit bridged by two $cbht^{2-}$ ligands in a centrosymmetric trimer [U(2) is the center of symmetry]. Each of the uranyl group, $U(1)O_2^{2+}$ and its symmetry-related $U(1A)O_2^{2+}$, is bonded to a tridentate $cbht^{2-}$ ligand through two deprotonated hydroxylamine hydroxyls and the central triazine nitrogen atom while both are bridged to each other through the $U(2)O_2^{2+}$ group and with the hydroxylamine hydroxyls of the two $cbht^{2-}$ ligated to U(2). The three uranium(VI) atoms are arranged in a linear fashion [U(1A)–U(2)–U(1) = 180°]. The trinuclear complex $(Et_3NH)_2[(U^{VI}O_2)_3(\mu\text{-bihyat})_2(bihyat)_2]$ has a linear arrangement similar to that of the three U^{VI} metal atoms.[13]

This mode of bridging action of $cbht^{2-}$ type ligands is the first example to be reported. The N atoms of the hydroxylamines in the $cbht^{2-}$ ligands of **3** have a flat trigonal geometry; therefore, they are sp^2-hybridized. This is in agreement with the ligands of **3**, **which** exhibits resonance structure B (Scheme 3). In marked contrast, in the complex $(Et_3NH)_2[(U^{VI}O_2)_3(\mu\text{-bihyat})_2(bihyat)_2]$, the N atoms of the bridged hydroxylamines have a trigonal pyramidal geometry; thus, they are sp^3-hybridized.[13]

The resonance structure B for complexes **1**–**3** is also supported by the short C(5)–N(6) bond distances [d_{mean} C(5)–N(6) ∼ 1.39 Å], revealing a double bond character. In addition, the carbazole moiety is coplanar with the triazine ring. The only exception is the plane defined by the carbazole of the bridging $cbht^{2-}$ in **3**, which forms an angle of 22.6° with the plane defined by triazine, accompanied by a 0.01 Å lengthening of the C(5)–N(6) bond.

The vanadium(V) centre in **4** adopts a distorted trigonal bipyramidal configuration (τ = 0.67; τ = {[O(3)–V(1)–O(4)] − [O(1)–V(1)–O(2)]}/60)[80] and is bonded to the $cbht^{2-}$ ligand through the triazine nitrogen N(3) [d(V–N_{tr}) = 1.997(2) Å], the two deprotonated hydroxylamine hydroxyl groups O(3) and O(4) [d_{mean}(V–O_h) = 1.993(2) Å] and two *cis* oxido groups O(1) and O(2) [d_{mean}(V═O) = 1.631(2) Å]. The vanadium(V) atom is displaced above the equatorial plane defined by two oxido groups and the triazine nitrogen atoms by 0.0216(3) Å. Similar to the crystal structure of **1**, the bond length of V–N_{tr} is one of the shortest reported in the literature [N(3)–V = 1.984 Å].

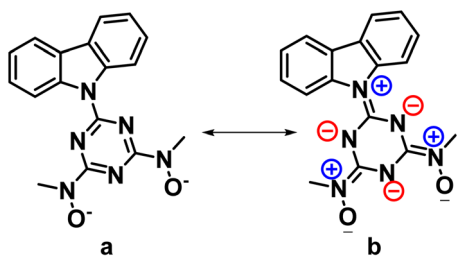

Scheme 3 Resonance structures of $cbht^{2-}$.

Table 1 Selected bond lengths between nitrogen and the hard metal ions such as U^{VI}, V^V and Fe^{III} of O–N–O tridentate ligands

Ligand/bond length (Å)	U^{VI}–N (1 : 1)	U^{VI}–N (1 : 2)	V^V–N (1 : 1)	Fe^{III}–N (1 : 1)	Fe^{III}–N (1 : 2)
$cbht^{2-}$	2.433(2)	2.530	1.977(2)	—	2.076(3)
$bihyat^{2-}$	2.436(4)[13]	2.518(5)[13]	1.993(3)[14]	—	1.976(2)[29]
qtn^{4-}	2.435(4)[31]	—	1.997(2)[31]	—	—
pdl^{4-}	2.441(6)[31]	—	2.005(2)[31]	—	—
enl^{4-}	—	—	1.992(3)[31]	—	—
$dipic^{2-}$	2.520(6)[84]	2.641(2)[84]	2.086(2)[85]		2.062(1)[86]
$Hpidiox^{2-}$	—	2.563[87]	1.988(5)[88]	2.005(8)[89]	2.030(1)[89]

Most of the five-coordinated vanadium(V) complexes have a square pyramidal geometry.[81–83] Strong σ-donor atoms in an *anti*-position to V═O cause distortion from square pyramidal to trigonal bipyramidal geometry by tilting the oxido groups; thus, the σ-donor and the oxido atoms avoid sharing the same orbital. The trigonal bipyramidal configuration of **4** confirms the strong-donating properties of the triazine heterocyclic N atom.

The coordination environment of Fe^{III} in **5** is a distorted octahedron with two $cbht^{2-}$ ligands bonded to the metal ion. Two hydroxylamine hydroxyls, O(1) and O(2), occupy the axial positions. The equatorial plane is defined by N_{tr}, two O_h donor atoms of one $cbht^{2-}$ ligand and the N_{tr} donor atom of the other $cbht^{2-}$ ligand. The Fe^{III} ion is 0.0781 Å above the equatorial plane. The mean Fe–O_h bond distance is 1.993 Å.

The M–N bond lengths of U^{VI}, V^V and Fe^{III}, similar to those of H_2cbht hard tridentate ligands, are shown in Table 1. It is apparent that the metal ion–N bond distances increase significantly, going from 1 : 1 to 1 : 2 (M : L) complexes.

In all crystal structures, the flat carbazole moiety forms strong π–π bonds with the triazine moiety of a neighboring molecule. The distances between the planes defined by the interacting carbazole and triazine range from 3.250 to 3.360 Å. In the crystal structure of **4**, π–π bonding arranges the molecules in a linear chain with π-interacting ligands inside and $V^VO_2^+$ moieties on the outside of the chain. The $V^VO_2^+$oxido moieties interact with the vanadium atoms of a neighboring chain, arranging the chains on infinite planes. In contrast to **4**, the crystal structures of **1**, **2**, **3** and **5** show π-interactions to be only between the two organic ligands of two different molecules, avoiding polymeric structures.

NMR spectroscopy

The organic molecules and complexes **1**–**4**·3H_2O were characterized using ^1H, ^{13}C and ^{51}V NMR (complex **4**) spectroscopy in DMSO-d_6 solutions. The ^1H and ^{13}C NMR spectra of the organic molecules are shown in Fig. S4–S7 (ESI†). The ^1H and ^{13}C chemical shifts of complexes **1**–**4**·3H_2O are listed in Table 2. For the DMSO-d_6 solutions of complex **1**, it was expected that the unidentate DMF and H_2O ligands in the coordination sphere of **1** would be replaced by DMSO-d_6. Thus, in the DMSO-d_6 solution, complex **1** is converted to $[U^{VI}O_2(cbht)(DMSO\text{-}d_6)_2]$. The ^1H NMR spectrum of the free ligand H_2cbht in DMSO-d_6 solution exhibited peaks at 3.45 and 7.40, 7.49, 8.17 and 9.14 ppm, which were

Table 2 ^{1}H and ^{13}C chemical shifts of complexes **1–4**·3H_2O. The ^{13}C of complexes **2** and **3** were calculated from the 2D {^{1}H, ^{13}C} HSQC spectra

Compound/^{1}H ppm (^{13}C ppm)	H(1)	H(5)	H(6)	H(7)	H(8)
H_2cbht	3.45(39.18)	8.17(119.60)	7.37(122.47)	7.49(125.22)	9.14(118.10)
1	3.80(38.20)	8.21(119.78)	7.40(122.12)	7.56(126.71)	8.96(117.34)
2	3.83(38.54)	8.21(119.78)	7.40(121.79)	7.56(126.42)	8.96(117.01)
3A + **3B**	3.83(38.54), 3.89(38.51), 4.60(41.35)	8.21(119.78), 8.20(119.68), 8.28(119.68)	7.40(121.79), 7.55(121.79), 7.38(121.79)	7.56(126.42), 7.66(126.36), 7.44(126.49)	8.96(117.01), 8.96(117.01), 9.01(117.01)
4	3.46(35.82)	8.21(119.74)	7.38(122.48)	7.53(126.85)	8.90(117.69)

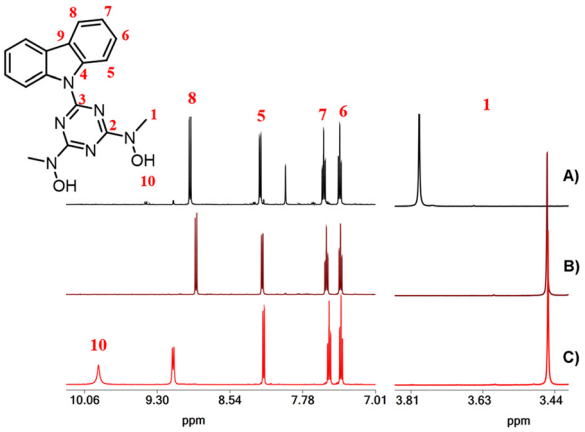

Fig. 3 ^{1}H NMR spectra of DMSO-d_6 solutions of (A) **1**, (B) **4**·3H_2O and (C) H_2cbht.

assigned to the methyl hydroxylamino and aromatic carbazole protons, respectively (Fig. 3). Upon complexation with the metal ions, the peaks are shifted to a lower field, except for the peak at 9.14 ppm [H(8)], which is shielded. The uranium(VI) ion causes a significantly larger shifting than vanadium(V), which is in line with the NMR spectra of complexes of the two metals with BHT-type ligands (Table 2).[31] The ^{51}V NMR spectrum of **4**·3H_2O in DMSO-d_6 exhibited broad peaks at −500 ppm, typical for this type of compound.[14,31]

The DMSO-d_6 solutions of a mixture of crystals of **2** and **3** exhibited peaks from the free ligand, **1**, **2** and **3**. This suggests that all compounds are in equilibrium in the solution. To further examine the reaction and correctly assign the ^{1}H NMR peaks, we reproduced the species in DMSO-d_6 solutions by reacting **1** with H_2cbht and Et_3N. The ^{1}H NMR spectrum of the solution confirmed the presence of the free ligand, **1**, **2** and **3** in equilibrium (eqn (1) and (2)). The addition of either Et_3N or H_2cbht drives the reaction to the right, increasing the concentrations of **2** and **3**, thus permitting the correct assignment of the peaks (Table 2).

$$[U^{VI}O_2(cbht)(DMSO\text{-}d_6)_2]\ (\mathbf{1}) + H_2cbht + Et_3N \rightleftharpoons [U^{VI}O_2(Hcbht)(cbht)]^{-}\ (\mathbf{2}) + Et_3NH^{+} \quad (1)$$

$$3[U^{VI}O_2(cbht)(DMSO\text{-}d_6)_2]\ (\mathbf{1}) + H_2cbht + 2Et_3N \rightleftharpoons [U^{VI}_3O_6(\mu\text{-}cbht)_2(cbht)_2]^{2-}\ (\mathbf{3}) + 2Et_3NH^{+} \quad (2)$$

Compound **2** exhibited a peak at 3.83 ppm, which was assigned to the methyl protons of methylhydroxylamine. The chemical shifts of the carbazole protons of **2** were the same as those of **1**. In the aromatic region, Complex **3** exhibited three

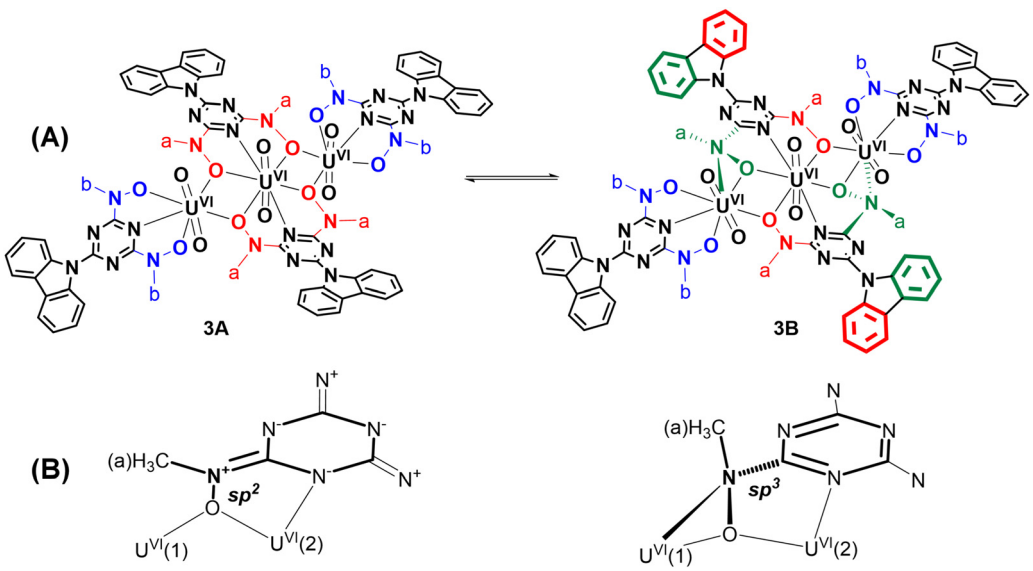

Scheme 4 (A) Equilibrium between tautomers **3A** and **3B**, and (B) sp^2 and sp^3 N structures.

peaks for the methylhydroxylamine protons at 3.83, 3.89 and 4.60 ppm. However, the highly symmetric crystal structure of **3** shows only two types of $-CH_3$, Ha and Hb (Scheme 4(A), molecule **3A**). The ratio of the integral of the peak at 3.89 ppm *vs.* the peak at 4.60 ppm is constant at 2.2, independent of the experimental conditions. Complex **3**, which is similar to the trinuclear complex $[U^{VI}{}_3O_6(\mu\text{-bihyat})_2(\text{bihyat})_2]^{2-}$, crystallizes with two N-hydroxylamine atoms in sp^3 instead of sp^2 hybridization. The $-CH_3$ attached to the sp^3 N is more deshielded than those on the sp^2 N atom. The shift in the ^{1}H NMR peaks of the $-CH_3$ groups supports equilibrium between species **3A** and **3B,** as shown in Scheme 4. The aliphatic region of the EXSY spectrum exhibited off-diagonal peaks between (i) the $-CH_3$ peak of **2** + H(b) of **3** and the $-CH_3$ peak of the free ligand and (ii) the peaks at 3.89 and 4.60 ppm. The former exchange process occurred between the ligands of **3** and the free ligand. The exchange between the $cbht^{2-}$ of **2** and the free ligand is not supported based on the fact that the exchange between **2** and **1** was not observed. The off-diagonal cross-peaks between the peaks at 3.89 and 4.60 ppm are much more intense than the exchange peaks of **3** with the free ligand, indicating a much faster intramolecular exchange process. Intramolecular changes in the structure of the hydroxylamine nitrogen atom from flat trigonal sp^2 to tetrahedral sp^3 are the only processes that do not require intermolecular exchange with the free ligand. Furthermore, the carbazole protons of the bridging $cbht^{2-}$ in **3B** should be asymmetric. The 2D $\{^1H\}$ COSY and EXSY (Fig. 4 and Fig. S8, ESI†) of the aromatic region show that the carbazole proton peaks split due to the asymmetry of the ligand and fast exchange. Apparently, the NMR results confirm that **3** in DMSO-d_6 solutions exists in the form of two fast-exchanging tautomeric forms, **3A** and **3B**.

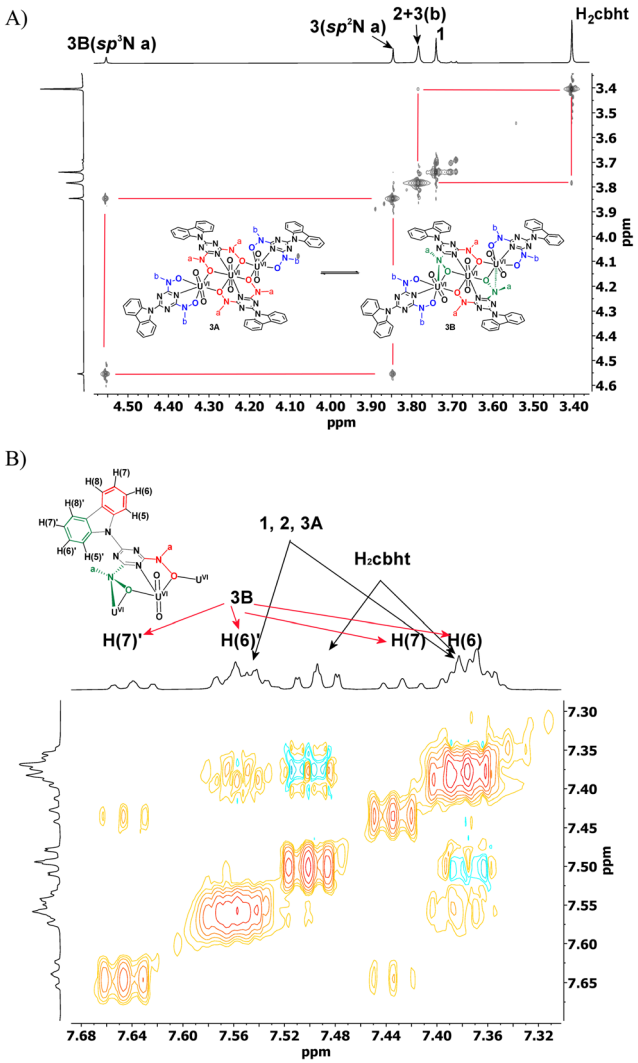

Fig. 4 (A) 2D $\{^1H\}$ grEXSY spectrum of the aliphatic region and (B) 2D $\{^1H\}$ grEXSY spectrum of part of the aromatic region of a DMSO-d_6 solution of **1** (6.00 μmol), H_2cbht (6.0 μmol) and triethylamine (72 μmol).

Luminescence and UV-vis

The luminescence and UV-vis data of the DMSO solution of the ligand and complexes **1**, **4**·3H_2O and **5**·9H_2O are listed in Table 3. Solutions of the free ligand H_2cbht in DMSO emit blue light after excitation at 338 nm (Fig. S9, ESI†). The shape of the emission spectrum (two peaks at 348 and 364 nm) is the same as that of carbazole (two peaks at 338 and 351 nm), slightly shifted at lower energies. The DMSO solutions of the complexes did not emit light.

The UV-vis spectrum of the DMSO solution of H_2cbht showed strong peaks at 276, 291 (sh), 312 and 323 nm. The shoulder at 290 nm originates from triazine intra-ligand electronic transitions, which are commonly observed in triazines without the chromophore.[31] The peak at 323 nm is assigned to carbazole intra-ligand transitions. In addition to the peak at 323 nm, the UV-vis spectrum of the non-substituted carbazole shows a peak at 336 nm. In H_2cbht, this peak collapsed into a broad shoulder (~335 nm).

The solution of **1** exhibited a LMCT peak at 326 nm, in addition to the ligand peaks. The intensity of the UV-vis peaks of the bound ligand of **4**·3H_2O in the solution increased by 50% compared to the spectrum of the solution of the free ligand and shifted slightly to higher wavelengths. A broad signal at

Table 3 UV-Vis data for the H_2cbht ligand and complexes **1**, **4**·3H_2O and **5**·9H_2O. The spectra were acquired in DMSO (ε units is M^{-1} cm^{-1})

	Intra-ligand transitions								CT	
Compound/peak	ε	nm	ε	nm	ε	nm	ε	nm	ε	nm
H_2cbht	6.0×10^4	276	4.2×10^4	291	2.3×10^4	312	2.9×10^4	323	—	—
1	6.7×10^4	272	5.5×10^4	288	2.9×10^4	315	3.1×10^4	323	3.1×10^4	326
4·3H_2O	6.3×10^4	276	4.8×10^4	291	3.8×10^4	313	4.8×10^4	325	—	—
5·9H_2O	6.7×10^4	277	5.5×10^4	291	3.4×10^4	314	3.9×10^4	325	3.6×10^3	540

320–380 nm was assigned to LMCT transitions. The CT transition of **5**·9H_2O appeared as a broad peak at 540 nm and is responsible for the deep purple colour of the complex.

Titration of 7.42×10^{-5} M H_2cbht with the metal ions shows a linear increase of CT transitions with increasing concentration of the metal ion. The absorption of $U^{VI}O_2^{2+}$ and $V^{V}O_4^{3-}$ with H_2cbht is maximum when the ratio between the metal ions and ligand is 1 : 1 (Fig. S10 and S11, ESI†). This agrees with the ^{1}H NMR experiments, showing the 1 : 1 species to be the most stable at these conditions. In contrast, regarding the Fe^{III} complex, the 1 : 2 metal to ligand species is stable in solution (Fig. S12, ESI†), suggesting that the crystallographically characterized complex **5**·9H_2O is the main species.

Electrochemistry

The cyclic voltammographs (CVs) of **1**, **4**·3H_2O and **5**·9H_2O are shown in Fig. 5. All complexes show ligand-centred oxidation waves at 886, 968 and 653 mV *vs.* NHE for **1**, **4**·3H_2O and **5**·9H_2O, respectively. The oxidation of the ligand on the electrode surface results in the emergence of daughter peaks at −474 and 136 mV *vs.* NHE for **1** and **4**·3H_2O, respectively, assigned to the reduction of the oxidized ligand. Interestingly, the potential for the oxidation of the ligand is linear and analogous to the energy of the LMCT transitions of the complexes (Fig. S13, ESI†).

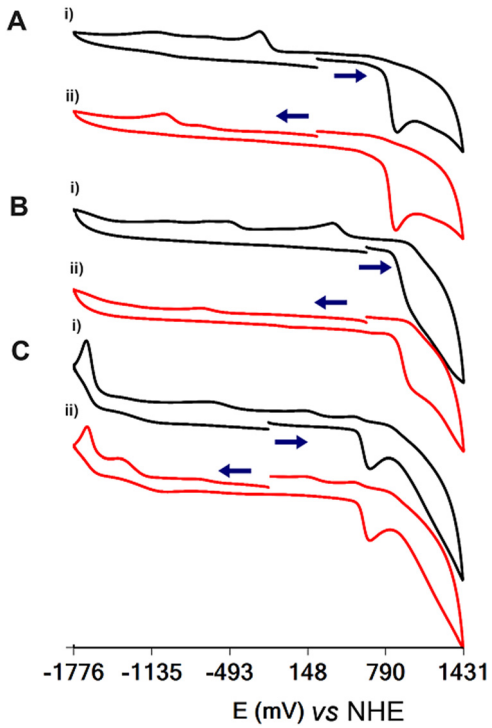

Fig. 5 Cyclic voltammograms of DMSO : H_2O (9 : 1) solutions of (A) **1** (1.00 mM), (B) **4**·3H_2O (1.00 mM) and (C) **5**·9H_2O (1.00 mM). (i) The scan starts towards a higher voltage and (ii) the scan starts towards a lower voltage. The supporting electrolyte is 0.1 M But_4NClO_4. Glassy carbon was used as the working electrode, platinum wire as the auxiliary electrode and Ag/AgCl (0.20 V *vs.* NHE) as the reference electrode.

In addition to the oxidation of the ligand, the CVs show an irreversible wave assigned to the metal-centred reduction of the complexes at −1015, −729 and −1666 mV *vs.* NHE for **1**, **4**·3H_2O and **5**·9H_2O, respectively.

Affinity of H_2cbht for $V^{V}O_4^{3-}$ and $U^{VI}O_2^{2+}$ based on ^{1}H NMR spectroscopy and square wave voltammetry (SWV)

The ^{1}H NMR spectra of the titration of a DMSO-d_6 solution of **4**·3H_2O with $U^{VI}O_2^{2+}$ are shown in Fig. 6. The addition of $U^{VI}O_2^{2+}$ to DMSO-d_6 solutions of **4**·3H_2O results in the disappearance of the peak of the hydroxylamine methyl protons of **4**·3H_2O and the appearance of a peak at 3.76 ppm assigned to **1** and a broad peak at 3.495 ppm. The ^{51}V NMR spectra of the solutions of **4**·3H_2O show that its peak at −500 ppm is replaced by a broad peak at −542 ppm (assigned to inorganic vanadate, Fig. S14, ESI†) after addition of $U^{VI}O_2^{2+}$.

The titration of DMF solutions of **4**·3H_2O with $U^{VI}O_2^{2+}$ was monitored using SWV (Fig. 7). Inorganic $U^{VI}O_2^{2+}$ in DMF solutions gives two reduction waves at −310 mV and −750 mV *vs.* NHE, which can be separated easily from the reduction peak of **1** at −972 mV *vs.* NHE. The addition of $U^{V}O_2^{2+}$ to the solution of **4**·3H_2O resulted in the appearance of a peak at −972 mV, suggesting the formation of complex **1** in line with the ^{1}H NMR results. However, the SWV also reveals the presence of inorganic $U^{VI}O_2^{2+}$ (Fig. 7). The presence of inorganic uranyl and vanadate in the solution indicates that the peak at 3.50 ppm originated from an inorganic $U^{V}O_2^{2+}$–$V^{V}O_4^{3-}$ salt, which interacts weakly with H_2cbht.[13]

The experiments reveal that H_2cbht, under acidic conditions, is selective toward ligation to $U^{V}O_2^{2+}$ and confirms that H_2cbht prefers to ligate $U^{VI}O_2^{2+}$ over $V^{V}O_4^{3-}$ similar to H_2bihyat.[13] In addition, the $U^{V}O_2^{2+}$–$V^{V}O_4^{3-}$ salt formation in H_2cbht–$U^{V}O_2^{2+}$–$V^{V}O_4^{3-}$ organic solutions is similar to the salt formed in H_2bihyat–$U^{V}O_2^{2+}$–$V^{V}O_4^{3-}$ aqueous solutions.[13]

The ^{1}H NMR spectra of a DMSO-d_6 solution of **4**·3H_2O (2.5 μmol), 2.5 μmol $U^{VI}O_2^{2+}$ and 5.0 μmol Et_3N show only

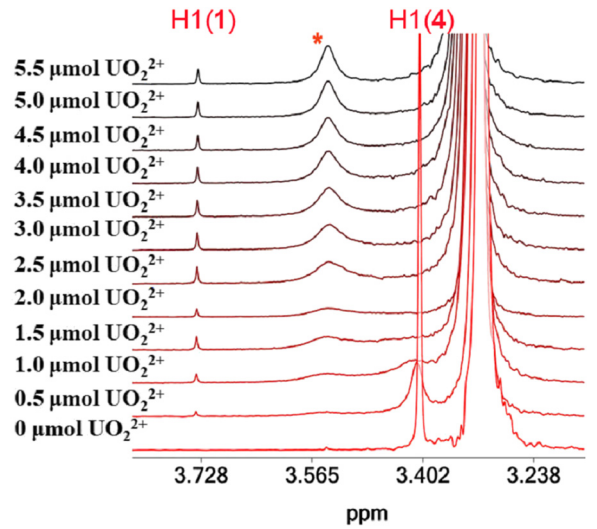

Fig. 6 The aliphatic region of the ^{1}H NMR spectra of solutions (DMSO-d_6) containing **4**·3H_2O (2.27 μmol) and $U^{VI}O_2^{2+}$ (0–5.5 μmol).

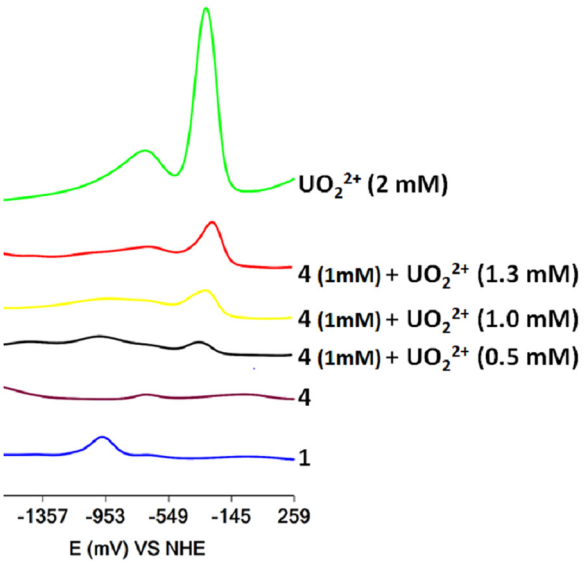

Fig. 7 Square wave voltammograms of DMF solutions of complex **4**·3H_2O (1 mM) and portions of $U^{VI}O_2^{2+}$ (0–1.3 mM). The supporting electrolyte is 0.1 M But_4NClO_4. Glassy carbon was used as the working electrode, platinum wire as the auxiliary electrode and Ag/AgCl (0.20 V *vs.* NHE) as the reference electrode.

two methyl peaks assigned to **1** and **4**·3H_2O. The integrals of the two peaks are equal, suggesting that the ligand H_2cbht, under alkaline conditions, binds $U^{VI}O_2^{2+}$ and $V^{V}O_2^{+}$ with the same strength. Moreover, yellow solid precipitates and the ^{51}V NMR spectrum of the solution show only the presence of complex **4**·3H_2O. The absence of a signal due to the released vanadate indicates that it forms a mixed $U^{VI}O_2^{2+}$–$V^{V}O_4^{3-}$ yellow salt that precipitates out.[31]

Quantification of $U^{VI}O_2^{2+}$, $V^{V}O_4^{3-}$ and Fe^{III} based on luminescence experiments

The quenching of the luminescence of the ligand by the addition of the hard metal ions $U^{VI}O_2^{2+}$, $V^{V}O_4^{3-}$ and Fe^{III} was measured, and the data were fitted using the Stern–Volmer equation $F_0/F = 1 + [M^{n+}] \times K_{SV}$, where F_0 is the luminescence of the ligand, F is the measured luminescence after the addition of the metal ion, $[M^{n+}]$ is the concentration of the metal ion, and K_{SV} is the quenching constant (Fig. 8). Both $U^{VI}O_2^{2+}$ and $V^{V}O_4^{3-}$ exhibit the same K_{SV} of 10×10^3 mol^{-1} L. The K_{SV} for Fe^{III} is doubled compared with that of $U^{VI}O_2^{2+}$ and $V^{V}O_4^{3-}$, presumably due to the paramagnetism of Fe^{III}.[50] However, the luminescence data at an analyte concentration above 4×10^{-5} M show an upward curvature, which is attributed to

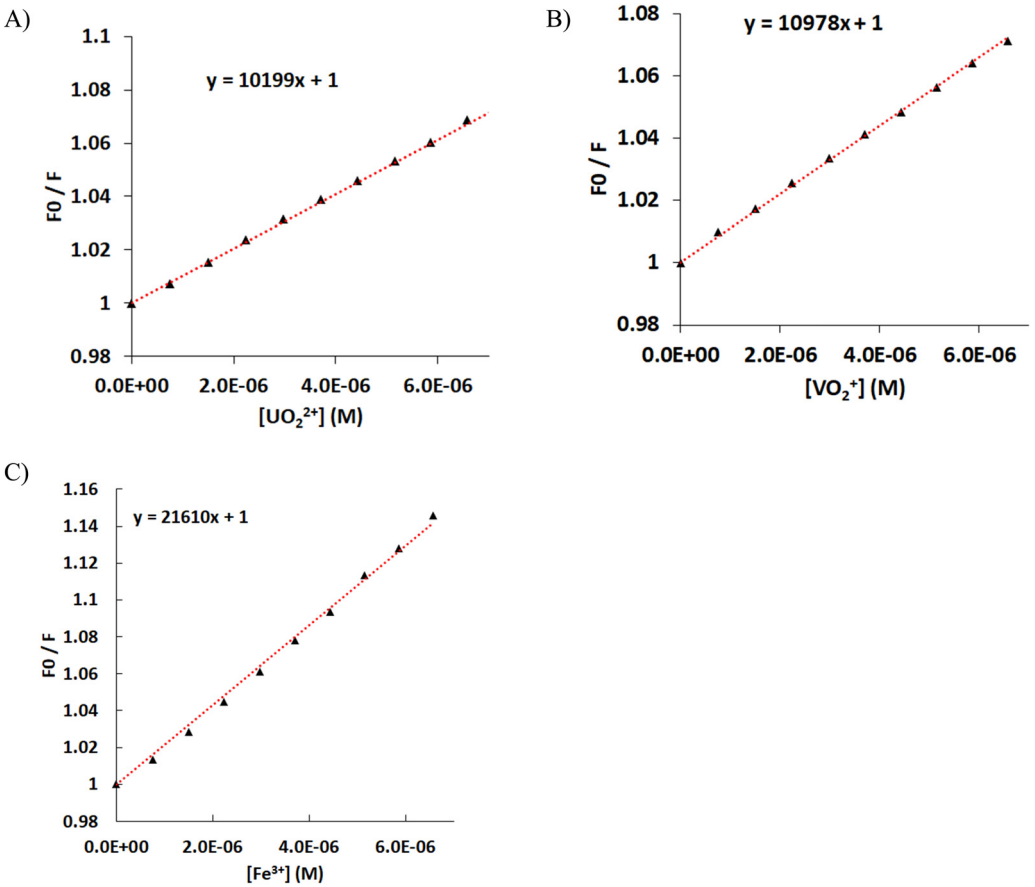

Fig. 8 Stern–Volmer plots of H_2cbht (3.74×10^{-5} M) and Et_3N (14.8×10^{-5} M) DMSO 9 : 1 H_2O solution after the addition of (A) $U^{VI}O_2^{2+}$, (B) $V^{V}O_4^{3-}$, and (C) Fe^{III}. The data were fitted using the equation $F_0/F = 1 + [M^{n+}] \times K_{SV}$.

the formation of the 1:2 Fe^{III}–$cbht^{2-}$ complex in solution.[90] The increase of e K_{SV} with the number of the ligands ligating a single metal ion indicates that the quenching of H_2cbht luminescence is initiated by the complexation with metal ions; therefore, the quenching follows a static than a collisional mechanism. The mechanism is also confirmed by the significant UV-vis changes in the absorption peaks during the titration of H_2cbht with metal ions.[91]

The association constant of the complexes was determined by the Benesi–Hildebrand method using fluorescence quenching data.[35,92] The Benesi–Hildebrand equation of a 1:1 complex is $1/(F_0 - F) = 1/\{(F_0 - F_\infty)K[M^{n+}]\} + 1/(F_0 - F_\infty)$, where F_0 is the luminescence of the ligand, F_∞ is the luminescence of the complex, F is the measured luminescence after the addition of the metal ion, $[M^{n+}]$ is the concentration of the metal ion, and K is the association constant. The Benesi–Hildebrand plots of $1/(F_0 - F)$ *vs.* $1/[M^{n+}]$ are straight lines (Fig. S15, ESI†), confirming that all metal complexes at concentrations of analyte below 4×10^{-5} are 1:1 in solution.

The $\log_{10}(K)$ values for $U^{VI}O_2^{2+}$, $V^{V}O_4^{3-}$ and Fe^{III} 1:1 metal to ligand complexes were found to be 4.61, 4.72 and 4.59, respectively.

The quantification (LOQ) limits were calculated from the Stern–Volmer graphs and were found to be 8.9×10^{-7}, 6.3×10^{-7} and 5.5×10^{-7} M for $U^{VI}O_2^{2+}$, $V^{V}O_4^{3-}$ and Fe^{III}, respectively. These values are in good agreement with the LOQ of other spectroscopic reagents, such as arsenazo, a typical spectroscopic reagent used for the quantification of $U^{VI}O_2^{2+}$.

Conclusions

In this work, we have demonstrated the design and synthesis of a spectroscopically labelled BHT-type ligand (H_2cbht). The $U^{VI}O_2^{2+}$ reaction with H_2cbht results in the synthesis of the mononuclear 1:1, 1:2, and trinuclear 3:4 metal-to-ligand complexes. The structural motifs of **2** and **3** were first observed for complexes of $U^{VI}O_2^{2+}$ with BHT-type ligands. $V^{V}O_2^{+}$ complexes with H_2cbht form trigonal bipyramidal structures instead of the expected square pyramidal structure, revealing the strong electron-donating ability of the triazine nitrogen donor atom. The 1:1 metal to ligand structures of $U^{VI}O_2^{2+}$ and $V^{V}O_2^{+}$ and the crystallographically characterized 1:2 structure of Fe^{III} were found to be the most stable in solution. ^{1}H and ^{51}V NMR spectroscopies and electrochemistry show that the ligand exhibits selectivity towards the coordination of uranium(VI) ions compared with vanadate in acidic organic solutions. In alkaline solutions, the binding strengths of H_2cbht for both V^{V} and U^{VI} are the same. In this study, based on the quenching of the luminescence of BHT-type ligands upon ligation with metal ions, we have demonstrated for the first time that the quantification of hard metal ions has good repeatability, with low a LOQ (at nM concentration level). The high strength of BHT-type ligands in binding hard metal ions makes them ideal probes for the detection of $U^{VI}O_2^{2+}$, $V^{V}O_2^{+}$ and Fe^{III}. It is expected that the quantification limits of the hard metal ions using BHT chelators can reach values <1 nM, indicating that the binucleated BHT ligands[31] form far more stable complexes than the mononucleated ones. Further work is underway to synthesize water-soluble binucleating BHT ligands to improve the LOQs and selectivity of the ligands for hard metal ions.

Author contributions

Angelos Amoiridis: formal analysis, investigation, validation, and writing – original draft. Michael Papanikolaou: formal analysis, investigation, and validation. Chryssoula Drouza: conceptualization, data curation, funding acquisition, methodology, and writing – review & editing. Themistoklis A. Kabanos: conceptualization and writing – review & editing. Anastasios D. Keramidas: conceptualization, data curation, funding acquisition, methodology, project administration, supervision, visualization, writing – original draft, and writing – review & editing.

Data availability

The rest of the data are presented in the manuscript and ESI,† and hard copies are available from the authors on reasonable request.

Conflicts of interest

There are no conflicts to declare.

Acknowledgements

This research was funded by the European Regional Development Fund and the Republic of Cyprus through the Research and Innovation Foundation (project: EXCELLENCE/0421/0520).

Notes and references

1 L. Février, F. Coppin, S. Pierrisnard, M. Bourdillon, L. V. Nguyen, N. Zaiter, S. Brandès, V. Sladkov, J. C. Chambron and M. Meyer, *J. Environ. Radioact.*, 2021, **235–236**, 106645.
2 M. E. Kirby, J. L. Sonnenberg, A. Simperler and D. J. Weiss, *J. Phys. Chem. A*, 2020, **124**, 2460–2472.
3 A. S. Ivanov, B. F. Parker, Z. Zhang, B. Aguila, Q. Sun, S. Ma, S. Jansone-Popova, J. Arnold, R. T. Mayes, S. Dai, V. S. Bryantsev, L. Rao and I. Popovs, *Nat. Commun.*, 2019, **10**, 819.
4 G. J. P. Deblonde, A. Ricano and R. J. Abergel, *Nat. Commun.*, 2019, **10**, 2438.
5 A. Sornosa-Ten, P. Jewula, T. Fodor, S. Brandès, V. Sladkov, Y. Rousselin, C. Stern, J. C. Chambron and M. Meyer, *New J. Chem.*, 2018, **42**, 7765–7779.
6 M. K. Lawson, M. Valko, M. T. D. Cronin and K. Jomová, *Curr. Pharmacol. Rep.*, 2016, **2**, 271–280.
7 L. Mullen, C. Gong and K. Czerwinski, *J. Radioanal. Nucl. Chem.*, 2007, **273**, 683–688.
8 P. W. Durbin, B. Kullgren, J. Xu and K. N. Raymond, *Health Phys.*, 1997, **72**, 865–879.

9 C. X. Bullock, C. S. Jamieson, P. Moënne-Loccoz, B. Taylor, J. A. M. Gonzalez, E. A. Draves and L. Y. Kuo, *Inorg. Chem.*, 2021, **60**, 7762–7772.
10 M. Stylianou, V. A. Nikolakis, G. I. Chilas, T. Jakusch, T. Vaimakis, T. Kiss, M. P. Sigalas, A. D. Keramidas and T. A. Kabanos, *Inorg. Chem.*, 2012, **51**, 13138–13147.
11 E. Y. Tshuva and D. Peri, *Coord. Chem. Rev.*, 2009, **253**, 2098–2115.
12 T. Hermon and E. Y. Tshuva, *J. Org. Chem.*, 2008, **73**, 5953–5958.
13 S. Hadjithoma, M. G. Papanikolaou, E. Leontidis, T. A. Kabanos and A. D. Keramidas, *Inorg. Chem.*, 2018, **57**, 7631–7643.
14 V. A. Nikolakis, J. T. Tsalavoutis, M. Stylianou, E. Evgeniou, T. Jakusch, A. Melman, M. P. Sigalas, T. Kiss, A. D. Keramidas and T. A. Kabanos, *Inorg. Chem.*, 2008, **47**, 11698–11710.
15 D. Fan and Q. Fang, *Int. J. Pharm.*, 2021, **597**, 120306.
16 L. Götzke, G. Schaper, J. März, P. Kaden, N. Huittinen, T. Stumpf, K. K. K. Kammerlander, E. Brunner, P. Hahn, A. Mehnert, B. Kersting, T. Henle, L. F. Lindoy, G. Zanoni and J. J. Weigand, *Coord. Chem. Rev.*, 2019, **386**, 267–309.
17 L. O. De Serrano, *Biomol. Concepts*, 2017, **8**, 169–178.
18 C. Drouza, V. Gramlich, M. P. Sigalas, I. Pashalidis and A. D. Keramidas, *Inorg. Chem.*, 2004, **43**, 8336–8345.
19 S. W. Smith, *J. Med. Toxicol.*, 2013, **9**, 355–369.
20 P. W. Durbin, *Health Phys.*, 2008, **95**, 465–492.
21 R. J. Abergel, P. W. Durbin, B. Kullgren, S. N. Ebbe, J. Xu, P. Y. Chang, D. I. Bunin, E. A. Blakely, K. A. Bjornstad, C. J. Rosen, D. K. Shuh and K. N. Raymond, *Health Phys.*, 2010, **99**, 401–407.
22 G. Szigethy and K. N. Raymond, *Inorg. Chem.*, 2010, **49**, 6755–6765.
23 G. Szigethy and K. N. Raymond, *Inorg. Chem.*, 2009, **48**, 11489–11491.
24 C. J. Sunderland, M. Botta, S. Aime and K. N. Raymond, *Inorg. Chem.*, 2001, **40**, 6746–6756.
25 S. T. Tsantis, D. I. Tzimopoulos, M. Holyńska and S. P. Perlepes, *Int. J. Mol. Sci.*, 2020, **21**, 555.
26 G. Szigethy and K. N. Raymond, *Chem. – Eur. J.*, 2011, **17**, 1818–1827.
27 O. A. Osin, S. Lin, B. S. Gelfand, S. L. J. Lee, S. Lin and G. K. H. Shimizu, *Nat. Commun.*, 2024, **15**, 2614.
28 I. Ekeltchik, J. Gun, O. Lev, R. Shelkov and A. Melman, *Dalton Trans.*, 2006, 1285–1293.
29 J. Gun, I. Ekeltchik, O. Lev, R. Shelko and A. Melman, *Chem. Commun.*, 2005, 5319–5321, DOI: **10.1039/b508138f**.
30 D. Sun, G. Melman, N. J. LeTourneau, A. M. Hays and A. Melman, *Bioorg. Med. Chem. Lett.*, 2010, **20**, 458–460.
31 A. Amoiridis, M. Papanikolaou, M. Vlasiou, N. A. G. Bandeira, H. N. Miras, T. Kabanos and A. Keramidas, *Inorg. Chem.*, 2023, **62**, 19971–19985.
32 X. Wu, Q. Huang, Y. Mao, X. Wang, Y. Wang, Q. Hu, H. Wang and X. Wang, *TrAC, Trends Anal. Chem.*, 2019, **118**, 89–111.
33 E. V. Gogol, E. S. Denisov, I. V. Lunev, O. S. Egorova, L. Sharipova and Y. A. Gusev, *IOP Conf. Ser. Mater. Sci. Eng.*, 2017, **225**, 012251.
34 S. Badakhshan, S. Ahmadzadeh, A. Mohseni-Bandpei, M. Aghasi and A. Basiri, *BMC Chem.*, 2019, **13**, 131.
35 V. S. Jisha, A. J. Thomas and D. Ramaiah, *J. Org. Chem.*, 2009, **74**, 6667–6673.
36 A. P. de Silva, H. Q. N. Gunaratne, T. Gunnlaugsson, A. J. M. Huxley, C. P. McCoy, J. T. Rademacher and T. E. Rice, *Chem. Rev.*, 1997, **97**, 1515–1566.
37 R. Martínez-Máñez and F. Sancenón, *Chem. Rev.*, 2003, **103**, 4419–4476.
38 A. B. Descalzo, R. Martínez-Máñez, R. Radeglia, K. Rurack and J. Soto, *J. Am. Chem. Soc.*, 2003, **125**, 3418–3419.
39 B. Valeur and I. Leray, *Coord. Chem. Rev.*, 2000, **205**, 3–40.
40 R. R. Avirah, K. Jyothish and D. Ramaiah, *Org. Lett.*, 2007, **9**, 121–124.
41 R. R. Avirah, K. Jyothish and D. Ramaiah, *J. Org. Chem.*, 2008, **73**, 274–279.
42 Y. Jia, D. Li and M. Hu, *Mater. Today Chem.*, 2023, **30**, 101518.
43 A. Hazra and P. Roy, *Anal. Chim. Acta*, 2022, **1193**, 339378.
44 T. Kajinehbaf and N. Alizadeh, *New J. Chem.*, 2022, **46**, 1763–1769.
45 V. G. Kanellis and C. G. dos Remedios, *Biophys. Rev.*, 2018, **10**, 1401–1414.
46 C. Varadaraju, G. Tamilselvan, I. V. M. V. Enoch, V. Srinivasadesikan, S.-L. Lee and P. M. Selvakumar, *New J. Chem.*, 2018, **42**, 3833–3839.
47 X.-A. Zhang and W.-D. Woggon, *J. Am. Chem. Soc.*, 2005, **127**, 14138–14139.
48 M. Wang, Z. Liu, X. Zhou, H. Xiao, Y. You and W. Huang, *Inorg. Chem.*, 2020, **59**, 18027–18034.
49 W. Liu, X. Dai, Z. Bai, Y. Wang, Z. Yang, L. Zhang, L. Xu, L. Chen, Y. Li, D. Gui, J. Diwu, J. Wang, R. Zhou, Z. Chai and S. Wang, *Environ. Sci. Technol.*, 2017, **51**, 3911–3921.
50 S. Pal, N. Chatterjee and P. K. Bharadwaj, *RSC Adv.*, 2014, **4**, 26585–26620.
51 D. Rehder, *Inorg. Chim. Acta*, 2020, **504**, 119445.
52 D. Rehder, *Inorganics*, 2023, **11**, 256.
53 D. Rehder, *Inorg. Chim. Acta*, 2023, **549**, 121387.
54 A. Rump, C. Hermann, A. Lamkowski, T. Popp and M. Port, *Arch. Toxicol.*, 2023, **97**, 1577–1598.
55 G. Xiao and J. Button, *J. Radioanal. Nucl. Chem.*, 2023, **332**, 185–191.
56 S. Liu, S. Wang, Y. Zhao, J. Li, C. Shu, Y. Li, J. Li, B. Lu, Z. Xu, Y. Ran and Y. Hao, *Chem. – Biol. Interact.*, 2023, **372**, 110356.
57 A. D. Keramidas, M. P. Rikkou, C. Drouza, C. P. Raptopoulou, A. Terzis and I. Pashalidis, *Radiochim. Acta*, 2002, **90**, 549–554.
58 J. C. Lee, H. B. Gray and J. R. Winkler, *J. Am. Chem. Soc.*, 2008, **130**, 6898–6899.
59 C. Deraeve, C. Boldron, A. Maraval, H. Mazarguil, H. Gornitzka, L. Vendier, M. Pitié and B. Meunier, *Chem. – Eur. J.*, 2008, **14**, 682–696.
60 D. C. Crans, A. D. Keramidas, H. Hoover-Litty, O. P. Anderson, M. M. Miller, L. M. Lemoine, S. Pleasic-Williams, M. Vandenberg, A. J. Rossomando and L. J. Sweet, *J. Am. Chem. Soc.*, 1997, **119**, 5447–5448.

61 K. Elvingson, A. D. Keramidas, D. C. Crans and L. Pettersson, *Inorg. Chem.*, 1998, **37**, 6153–6160.
62 S. B. Etcheverry, D. C. Crans, A. D. Keramidas and A. M. Cortizo, *Arch. Biochem. Biophys.*, 1997, **338**, 7–14.
63 I. Hadjiadamou, M. Vlasiou, S. Spanou, Y. Simos, G. Papanastasiou, E. Kontargiris, I. Dhima, V. Ragos, S. Karkabounas, C. Drouza and A. D. Keramidas, *J. Inorg. Biochem.*, 2020, **208**, 111074.
64 K. Ioannou, C. Eleftheriou, C. Drouza, K. S. Pafiti, T. Panayi, A. D. Keramidas, L. C. Zacharia and M. C. Vlasiou, *J. Mol. Struct.*, 2022, **1257**, 132582.
65 M. Loizou, P. Papaphilippou, M. Vlasiou, M. Spilia, D. Peschos, Y. V. Simos, A. D. Keramidas and C. Drouza, *J. Inorg. Biochem.*, 2022, **235**, 111911.
66 M. Aureliano, N. I. Gumerova, G. Sciortino, E. Garribba, C. C. McLauchlan, A. Rompel and D. C. Crans, *Coord. Chem. Rev.*, 2022, **454**, 214344.
67 D. C. Crans, N. E. Barkley, L. Montezinho and M. M. Castro, *RSC Metallobiol.*, 2019, **2019**, 169–195.
68 D. C. Crans, L. Henry, G. Cardiff and B. I. Posner, *Met. Ions Life Sci.*, 2019, **19**, 203–230.
69 A. L. De Sousa-Coelho, M. Aureliano, G. Fraqueza, G. Serrão, J. Gonçalves, I. Sánchez-Lombardo, W. Link and B. I. Ferreira, *J. Inorg. Biochem.*, 2022, **235**, 111915.
70 G. Ferraro, M. Paolillo, G. Sciortino, F. Pisanu, E. Garribba and A. Merlino, *Inorg. Chem.*, 2023, **62**, 8407–8417.
71 S. V. Gayakwad, D. S. Wankhede, V. D. Ragole, S. G. Wanale, S. A. Dake and S. B. Maulage, *Anti-Infective Agents*, 2023, **21**, 41–56.
72 C. Ghosh, D. Patra, N. Bala, I. Majumder, N. Sepay, P. Mukhopadhyay, S. Das, R. Kundu, M. G. B. Drew, A. R. León, T. Ghosh and M. Pradhan, *Biometals*, 2022, **35**, 499–517.
73 D. Rehder, *Comprehensive Inorganic Chemistry II: From Elements to Applications*, 2nd edn, 2013, vol. 3, pp. 819–834.
74 G. Sciortino, V. Ugone, D. Sanna, G. Lubinu, S. Ruggiu, J. D. Maréchal and E. Garribba, *Front. Chem.*, 2020, **8**, 345.
75 V. Ugone, D. Sanna, G. Sciortino, D. C. Crans and E. Garribba, *Inorg. Chem.*, 2020, **59**, 9739–9755.
76 K. Kostenkova, A. Levina, D. A. Walters, H. A. Murakami, P. A. Lay and D. C. Crans, *Chem. – Eur. J.*, 2023, **29**, e202302271.
77 A. Levina, A. Pires Vieira, A. Wijetunga, R. Kaur, J. T. Koehn, D. C. Crans and P. A. Lay, *Angew. Chem., Int. Ed.*, 2020, **59**, 15834–15838.
78 A. Levina, C. Uslan, H. Murakami, D. C. Crans and P. A. Lay, *Inorg. Chem.*, 2023, **62**, 17804–17817.
79 E. A. Ignatenko, A. A. Gorbunov, E. V. Shklyaeva and G. G. Abashev, *Chem. Heterocycl. Compd.*, 2014, **50**, 691–698.
80 A. W. Addison, T. N. Rao, J. Reedijk, J. Van Rijn and G. C. Verschoor, *J. Chem. Soc., Dalton Trans.*, 1984, 1349–1356, DOI: **10.1039/DT9840001349**.
81 D. Rehder, *J. Inorg. Biochem.*, 2008, **102**, 1152–1158.
82 D. C. Crans, M. L. Tarlton and C. C. McLauchlan, *Eur. J. Inorg. Chem.*, 2014, 4450–4468.
83 C. C. McLauchlan, B. J. Peters, G. R. Willsky and D. C. Crans, *Coord. Chem. Rev.*, 2015, **301–302**, 163–199.
84 J. M. Harrowfield, N. Lugan, G. H. Shahverdizadeh, A. A. Soudi and P. Thuéry, *Eur. J. Inorg. Chem.*, 2006, 389–396, DOI: **10.1002/ejic.200500671**.
85 B. S. Parajón-Costa, O. E. Piro, R. Pis-Diez, E. E. Castellano and A. C. González-Baró, *Polyhedron*, 2006, **25**, 2920–2928.
86 A. Pushpaveni, S. Packiaraj, S. Govindarajan, G. T. McCandless, C. F. Fronczek and F. R. Fronczek, *Inorg. Chim. Acta*, 2018, **471**, 537–549.
87 G. Tian, S. J. Teat, Z. Zhang and L. Rao, *Dalton Trans.*, 2012, **41**, 11579–11586.
88 C. J. Leggett, B. F. Parker, S. J. Teat, Z. Zhang, P. D. Dau, W. W. Lukens, S. M. Peterson, A. J. P. Cardenas, M. G. Warner, J. K. Gibson, J. Arnold and L. Rao, *Chem. Sci.*, 2016, **7**, 2775–2786.
89 X. Sun, C. Xu, G. Tian and L. Rao, *Dalton Trans.*, 2013, **42**, 14621–14627.
90 M. H. Gehlen, *J. Photochem. Photobiol., C*, 2020, **42**, 100338.
91 S. Bano, A. Mohd, A. A. P. Khan and K. S. Siddiqi, *J. Chem. Eng. Data*, 2010, **55**, 5759–5765.
92 H. A. Benesi and J. H. Hildebrand, *J. Am. Chem. Soc.*, 1949, **71**, 2703–2707.